ELSEVIER

Journal of Alloys and Compounds 419 (2006) 180–190

Journal of ALLOYS AND COMPOUNDS

www.elsevier.com/locate/jallcom

Thermal analysis and microscopical characterization of Al–Si hypereutectic alloys

F.C. Robles Hernández*, J.H. Sokolowski

Light Metals Casting Technology (LMCT) Group, Room 212A, Essex Hall, 401 Sunset Avenue, Windsor, Ont., Canada N9B 3P4

Received 1 June 2005; accepted 22 July 2005
Available online 5 December 2005

Abstract

In this research paper are presented the identified phases by thermal analysis and microscopy presented by four 3XX.X Al–Si hypereutectic alloys that were solidified under different conditions including natural heat exchange and quenching. In addition, a qualitative analysis of the phases was conducted by EDX scanning electron microscopy. The EDX results were used to identify the stoichiometry for the particular phases based on data reported in the literature. A total of nine reactions were detected by thermal analysis that were confirmed by optical and electron microscopy, where two additional phases (Fe and Pb enriched) were also detected. Above the liquidus temperature, the phase known as Si agglomerates was identified; the nature and principal characteristics of this phase are discussed in the present paper. Using thermal analysis, the phase identification, fraction solid and nucleation temperature for all the phases was conducted.

Keywords: Aluminium alloys; Quenching; Liquid phase; Silicon agglomerates

1. Introduction

The Al alloys is a group of casting materials that are in tonnage terms the second most popular after ferrous castings. The Al alloys have been divided into several systems that were identified based on their alloying elements by the American Aluminium Association (AAA). Aluminium-Silicon (Al–Si) alloys are the most abundant among cast alloys and have wide-spread applications, especially in the aerospace and automotive industries and are identified by the AAA as the 3XX.X series of aluminiums alloys that constitutes from 80 to 90% of the total Al castings produced world wide [1–3]. The dominant group of Al–Si foundry alloys contain between 5 and 25 wt.% Si, with Mg, Ni and Cu additions. It is important to mention that until now Fe has not been considered as an alloying element; however, current research conducted by the LMCT demonstrates the opportunities to control cast component integrity by optimizing Fe with Mn additions to transform the detrimental Fe enriched intermetallics from its typical *needle* shape into the less harmful *Chinese script* phase [1,5–9] and lowering the porosity level [10].

The presence of coarse primary Si particles in the microstructure of the Al–Si hypereutectic alloys has been identified as the main limitation for their industrial use. Even with the use of silicon modifiers and high cooling rates, the primary Si particles can only be reduced in size [11]. Nonetheless, Al–Si hypereutectic alloys have already been used in the automotive industry for engine blocks production (Vega 2300 engine), cylinder liners and pistons [6–9,12]. However, there are not reports of the performance of the Vega 2300 engine and is no longer available for regular production; which could be due to that the very hard primary Si particles certainly increase locally the wear resistance of the alloy, but unfortunately Si is brittle and is easy to crack exposing the soft Al matrix to extreme wear resulting catastrophic for the automotive or aerospace components [5,13–15]. The apparent solution to fully refine the primary Si particles are the liquid metal treatments that can modify the primary Si particles into fine Al–Si eutectic, that will contribute in a considerable increment of the wear resistance for these alloys [12,16].

Al–Si hypereutectic alloys for engine blocks or cylinder liners applications is the ideal solution to eliminate cast iron cylinder liners; additionally, Al–Si hypereutectic alloys possess low thermal expansion, excellent castability and low density which

* Corresponding author at: 7507 Wildfern Dr. Mississauga, Ont., Canada L4T 3P7. Tel.: +1 519 252 6728; fax: +1 514 370 3310.
E-mail address: fcrh20@yahoo.com (F.C. Robles Hernández).

0925-8388/$ – see front matter © 2005 Elsevier B.V. All rights reserved.
doi:10.1016/j.jallcom.2005.07.077

make them attractive for automotive and aerospace applications [13,17,18]. In contrast, the use of other materials such as cast iron cylinder liners for aluminiums engine blocks applications have the following disadvantages: several steps machining, formation of residual stresses, preheating of the cylinder liners for cast-in applications, additional steps for engine block production (press in) technique, cast iron is limited to air quenching in order to avoid corrosion, formation of harmful phases and interfaces between the Al engine block and the cylinder liner, low heat conductivity and high density, different machining conditions, to mention just a few [12,16].

Thermal analysis is a powerful tool that has been successfully used to determine characteristic temperatures, fraction solids and latent heats during the solidification process. Thermal analysis has been applied effectively for Al–Si hypoeutectic alloys [4,19–27]; however, the Al–Si hypereutectic alloys have not been as investigated. Bäkerud et al. [4] have reported the most complete characterization using thermal analysis and SEM/EDX for two 390 Al–Si hypereutectic alloys. However, a more detailed analysis is required in order to develop techniques that can contribute to the use of Al–Si hypereutectic alloys for wear resistant applications.

Due to the above-mentioned arguments, it is of crucial importance to conduct studies to understand the solidification pathways as well as liquid state characteristics of the Al–Si hypereutectic alloys. This will allow the development of novel technologies to fully refine the primary Si morphology, which in turn will increase the demand for the Al–Si hypereutectic alloys for wear resistance applications including the engine blocks, cylinder liners, brakes, clutches, etc. The present research investigation was conducted to understand in more detail the solidification pathways followed by the Al–Si hypereutectic alloys, nucleation temperature, fraction solid, microstructure and phases morphology among other characteristics. This can be used as a principle to determine the exact temperatures for chemical, mechanical, thermal, electromagnetic or combined techniques for the modification of the microstructure as well as the exact temperature determination for heat and/or solution treatments. By knowing the characteristics of the Si agglomerates, novel liquid and semi-solid melt treatments can be successfully developed and implemented [12,16,28–35].

2. Experimental methodology

Four Al–Si hypereutectic alloys were used for the present study; two of these alloys feel into the 390.1 AAA designation and the other two into the 393.2. The chemical composition of the above-mentioned alloys is presented in Table 1.

Ingots of 12 kg of the respective alloys were melted in a resistance furnace at a super heat (casting) temperature of 150 °C above liquidus. The alloys were held isothermally during the experiments. The melt was degassed blowing Ar gas by a degassing unit at a rate of 20 St. ft^3/h, through a graphite impeller at a rotating speed of 120 rpm for 20 min. After degassing, the hydrogen level was in all cases below 0.1 ± 0.005 mL H_2/100 g of aluminiums as measured using a calibrated AlSCAN unit.

After the hydrogen measurements were conducted, the molten alloys were poured into a stainless steel crucible with a capacity of 700 mL, which was then insulated on top and bottom using refractory bricks of alumina to minimize the gradient of temperatures. The poured samples had masses of 1300 ± 20 g of Al–Si hypereutectic alloy. Also, samples for each alloy composition were poured into a die-cast bar system (reaching cooling rates >2 °C/s that minimizes Si macrosegregation), these bars were machined to obtain cylindrical specimens with 15 mm in diameter by 16 mm in height with masses of 7.5 g. Both types of samples were solidified under natural heat exchange conditions for all the alloys. During solidification, a K thermocouple previously calibrated according to the standard of the National Institute of Standards and Technology (NIST) was inserted in the centre of the sample to record the cooling curve from the superheat temperature until 400 °C. The thermal analysis was conducted three times for every alloy composition and solidification conditions to ensure the quality of the results. The results presented are the average of all the thermal analysis measurements. Samples for the 390.1[a] and 393.2[a] alloys were quenched in a salt-water solution (H_2O + 15 wt.% NaCl) from various temperatures from above and below the liquidus temperature.

Table 1
Chemical composition (in wt.%) of the investigated Al–Si alloys and their calculated liquidus (T_{LIQ}) temperature using the Si equivalency method (Si_{EQ}) [12,36]

AAA designation	Si	Cu	Fe	Mg	Mn	Ni	Calculated T_{LIQ}
390.1[a]	13.14	4.11	0.51	0.99	0.21	2.19	600.2
390.1[b]	13.80	4.00	0.61	1.30	0.23	0.45	599.7
393.2[a]	25.0	1.18	0.39	0.05	0.12	0.4	752.5
393.2[b]	28.64	2.43	0.90	0.15	0.36	0.57	794.9

Sections of the analytical samples were cut parallel and in close proximity to the thermocouple for metallographic analysis. The metallographic samples were mounted in cold resin and polished following the standard metallographic procedures. Optical microscopy, scanning electron microscopy (SEM) and energy dispersive X-ray (EDX) spectroscopy were used for the identification of the phases. The stoichiometry of the phases was determined comparing the results of the EDX semi-quantitative chemical analysis with the results reported in the literature for alloys with similar composition.

3. Results and discussions

3.1. Thermal analysis

Fig. 2 shows the cooling, first derivative, baseline and fraction solid curves for the 390.1[a,b] and 393.2[a,b] Al–Si alloys as obtained from thermal analysis for the two types of samples. The first derivative of the cooling curve was determined to enhance slope changes that are related to the solidification reactions for the different phases; and facilitates the determination of the nucleation time, temperature, fraction solid and cooling rate of the phases. It is clear from this figure that both alloys present similar nucleation reactions and solidification characteristics, nonetheless, some differences that will be discussed were found. The use of the two thermal analysis methods allowed the precise determination of the characteristics for all the solidification reactions. For instance, using the small samples was assessed the exact temperature and fraction solid involved for the Si agglomerates; while for the Ni and Cu enriched phases, the thermal analysis conducted using the large samples was more appropriate.

The present investigation provides unique information for the solidification pathways followed by the Al–Si hypereutectic alloys; particularly, the identification of a reaction at temperatures above liquidus by thermal analysis and image analysis. This reaction can correspond to the transformation of the Si agglomerates into primary Si particles. The identification of this reaction was carried out using high-resolution thermal analysis

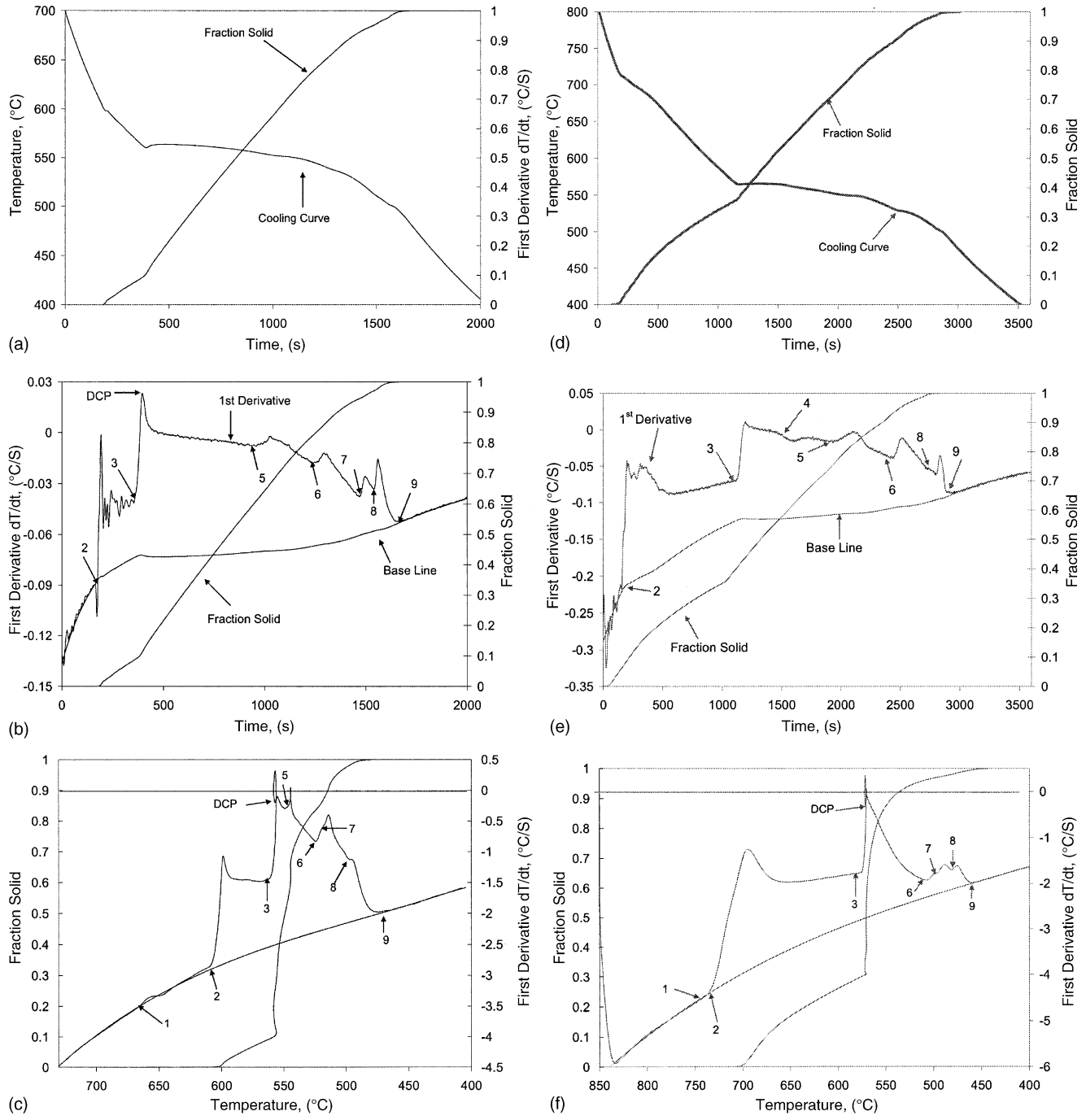

Fig. 1. Thermal analysis results for the 390.1[a] (a–c) and 393.2[a] (d–f) alloys solidified at low (a, b, d and e) and high cooling rates (c and f). Note the abrupt increase in fraction solid after the Al–Si eutectic reaction and Dendrite Coherency Point (DCP).

techniques and algorithms (Fig. 1a and d). The Si agglomerates nucleate at temperatures as high as 1075 °C and has a different crystalline structure than solid Si; as reported in the literature [29–35]. Due to the limitations of the equipment used for this research investigation, it was not possible to determine the nucleation temperature for the Si agglomerates; however, the above-mentioned reaction was detected at ∼666 °C on to the big samples for the 390.1[a] alloy.

In following are described the main differences among Al and Si that do not allow coherency among their crystalline structures that results in the non-dendritic microstructure of the alloy. The FCC crystalline structure of Al is an "*Al*" copper type with a lattice parameter $\alpha_{Al} = 4.0490$ Å, and an "*A4*" (diamond like) for Si with an $\alpha_{Si} = 5.4282$ Å [40]. The solidification process for Al is normal and for Si is layered (2D) [1]. In other words, during nucleation of Al, the Al atoms have no preferred locations to be attached. Conversely, the nucleation of Si atoms is carried out in an ordered manner where the Si atoms are attached at specific locations pilling up Si atoms until a line of atoms is full and then a set of lines that form an atomic plane that are pilled epithaxially

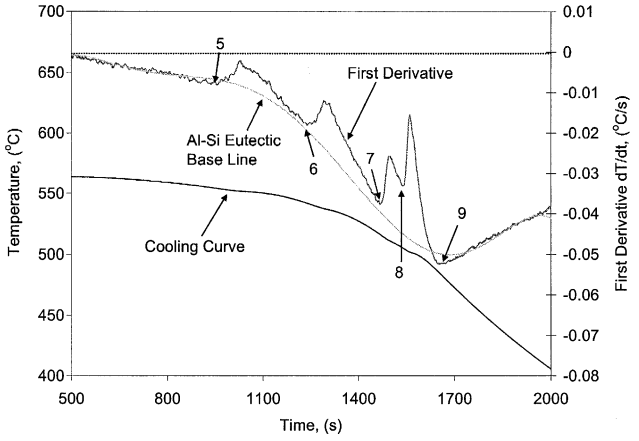

Fig. 2. Section of the cooling, first derivative and baseline curves for the Al–Si eutectic reaction of the 390.1[a] alloy solidified under natural heat exchange conditions to determine the *apparent fraction solid* (af_s) for the Mg, Ni and Cu enriched phases.

forming the primary Si and/or Si eutectic crystals that slows down the solidification process for Si [1]. The solidification of the Al enriched regions promote a rapid increase in fraction solid from the α-Al halo until the Al–Si eutectic [41]. The increment in fraction solid is from <10% to ~20% in only 4 °C and then a 40% increment is observed in 10 °C or less confirming the abrupt increment in the fraction solid observed in Fig. 1b, c, e and f.

Fig. 2 shows examples for the Si agglomerates on quenched samples at temperatures as high as 130 and 80 °C above the respective liquidus for the 390.1[a] and 393.2[a] Al–Si hypereutectic alloys; indicating that the Si agglomerates are formed at higher temperatures. The equivalent fraction "*solid*" related to the Si agglomerates to liquidus temperature as determined by thermal analysis for the 390.1[a] alloy was $fS_{Si}^{AGGL} = 0.065$ wt.% that is almost neglected. However, this phase plays a crucial role for the successful application of melt treatments at temperatures above liquidus, since by using electromagnetic stirring and vibration melt treatments, these particles can be fully refined that result in their full modification into refined Si eutectic particles [12].

In the first derivative for both types of alloys, 390.1[a,b] and 393.2[a,b], nine metallurgical reactions were identified as shown in Fig. 1 and are summarized in Table 2 with their corresponding stiochiometry; the identification numbers used in both, the figure and the table, indicate the same solidification reaction. In this particular case, it is crucial to precisely identify parameters such as temperature, since this accuracy is directly reflected in the precision to calculate the fraction solid and apparent fraction solid for a particular phase or all the phases.

Table 2
List of reactions and the Dendrite Coherency Point (DCP) identified by image analysis and thermal analysis in samples for the 390.1 and 393.2 Al–Si hypereutectic alloys

ID #	Description
1	"*Si Agglomerates*; *Transformation*"
2	Primary Si (liquidus)
3	Al–Si eutectic
4	$Al_{15}(Fe, Cr, Mn)_3Si_2$
DCP	Dendrite Coherency Point
5	Mg_2Si eutectic
6	Al_3Ni eutectic
7	Al_3CuNi eutectic
8	Al_2Cu eutectic
9	End of the solidification (solidus)

The cooling and first derivative curves for the 393.2[a,b] Al–Si hypereutectic alloys were found to be similar to each other; however, small differences in comparison to the 390.1[a,b] alloys were found. The main significant differences are the considerably higher liquidus temperature for the 393.2[a,b] alloys, solidification time, solidification range and fraction solids.

Djurdjevic et al. [37,39] and MacKay [38] reported that using thermal analysis, the af_s for the Mg, Ni, Cu enriched phases can be determined by calculating the baseline for the first derivative for the Al–Si eutectic reaction. Fig. 3 shows the methodology for the assessment of the "*apparent fraction solid* (af_s)" for the Mg, Ni, Cu enriched phases. The importance of the analysis of these phases is due to their strengthening effect that is usually enhanced and set by applying heat treatments that promote the precipitation of coherent or incoherent Mg, Ni, Cu enriched phases that improve the mechanical properties of Al–Si hypereutectic alloys.

Fig. 2 shows the Al–Si eutectic baseline that is a hypothetical model where only this reaction takes place and ends presumably at the solidus temperature [37]. Therefore, any increase in the amount of heat released (exothermic behaviour) was identified in the first derivative as nucleation of phases (such as points from 5–8) corresponding to the Mg, Ni or Cu enriched phases. The amount of exothermic heat released during the nucleation of a phase is proportional to the amount of precipitating phase, latent heat and enthalpy of transformation. Therefore, the prediction of the strengthening effect of the particular phase(s) can be assessed by determining the af_s for all the phases and relate to its contribution to the mechanical properties (hardness, micro-hardness, strength, creep, fatigue, etc.). The heat treatment conditions play an important role because the enhancement of the mechanical properties relays totally on the temperature and time of the treatment itself. Therefore, it is not simple to make a single algorithm for all Al–Si alloys and heat treatment conditions; however, the silicon equivalent (Si_{EQ}) methodology [36] is the alternative to develop a mathematical model of this nature and is currently in under investigation by the LMCT group. A summary of the temperatures and the fraction solids for all the solidification reactions for the 390.1[a,b] and 393.2[a,b] alloys solidified under the various solidification conditions is presented in Table 3.

The value of the af_s in an alloy with a constant composition and similar solidification conditions must be the same. Any change in the apparent fraction solid in a sample of the same melt, but distinct solidification conditions can be related to the amount of dissolved Mg, Ni and Cu elements within the matrix, the level of refinement of the microstructure or modification of this particular phase. For this reason, more than one thermal analysis techniques, solidification conditions and alloys composition were investigated.

The determination of the af_s for elements present in an alloy in the form of traces is difficult; however, these phases can also be studied by image analysis, which is not simpler. For this rea-

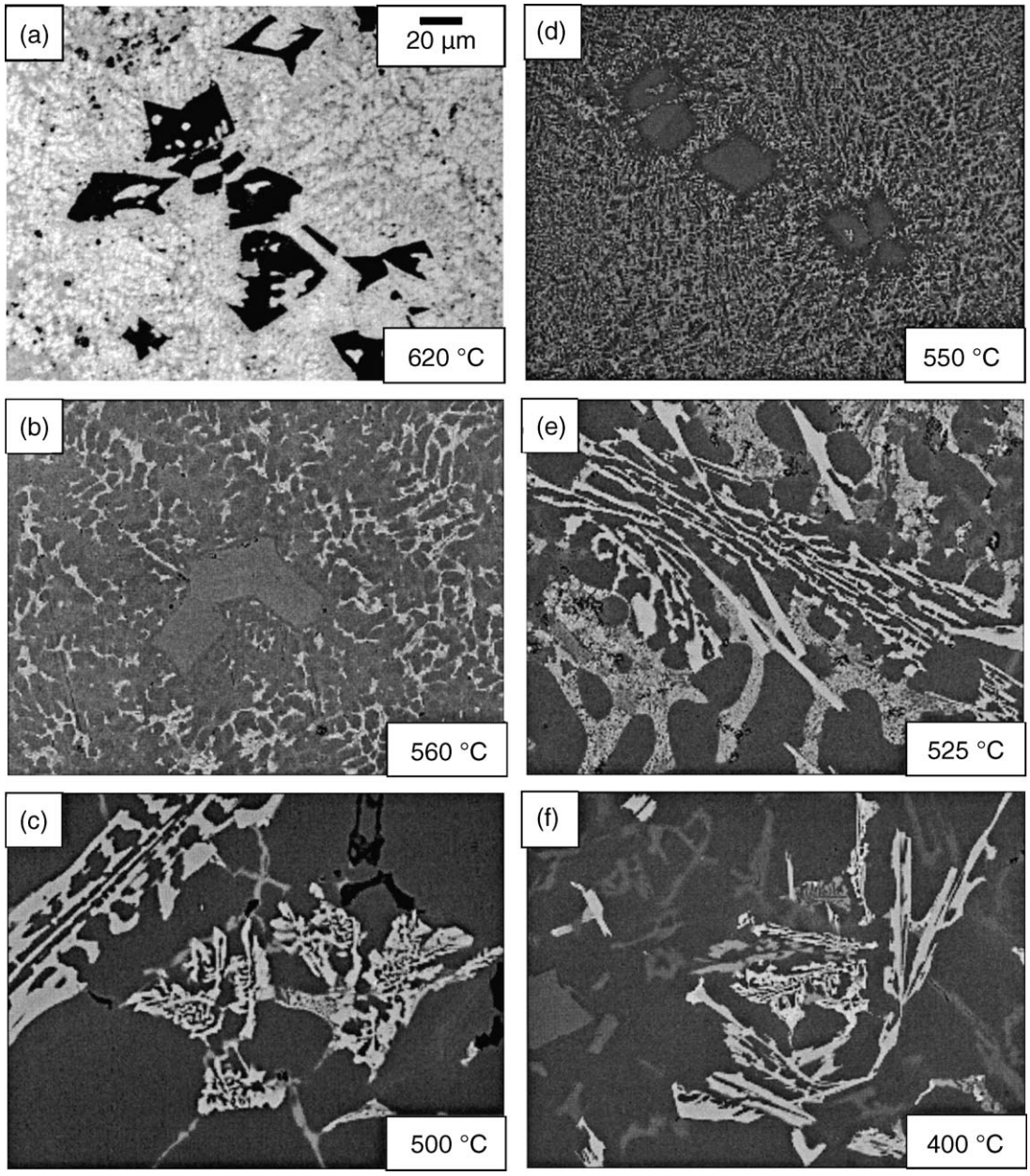

Fig. 3. Examples of optical and scanning electron micrographs for the 390.1[a,b] and 393.2[a,b] alloys quenched from different temperatures in liquid and semi-solid stages.

son, in the present research, the af_s for Pb, Sn, Ti, Sr, etc. is not reported alone, but rather together with Mg, Cu or Ni enriched phases (Fig. 3 and Table 3). However, an indirect methodology to determine the amounts of traces of elements present in an alloy and is based on the determination of the effect of these elements on the cooling curve and consequently first derivatives. For instance, Djurdjevic et al. [37,39] measure the undercooling of the α-Al reaction and developed an algorithm to predict the level of Si modification caused by additions of Sr to the molten metal. More recently, was found that elements such as lead, tin and bismuth have a significant influence in solidus temperature. Levels of these elements above 100 ppm decrease the solidus temperature in up to ∼20 °C. This results in a catastrophic practice, since by applying conventional heat treatments, considerable amounts of incipient melts can be formed, which in turn prevent the mechanical properties enhancement assed by heat treatments. Conversely, detrimental particles that act as stress concentrators are formed. An increment in the hydrogen level from 0.06 to 0.125 mL H_2/100g Al is responsible for a change in the nucleation reaction for the Cu enriched phases of >12 °C, which under certain conditions can increase the porosity levels in up to 400%.

Table 3 shows that for all alloys, the Si agglomerates "*transformation*" above the liquidus temperatures and was at higher temperatures in samples solidified at low cooling rates. It is of particular interest the lower fraction solid for the Al–Si eutectic for the samples solidified at high cooling rates; however, in

Table 3
Thermal analysis results for the temperature (°C) and fraction solid (%) for all the respective alloys solidified under different conditions

Alloy/reaction	1	2	3	DCP	5	6	7	8	9
Low cooling rate									
390.1[a]	660	600	562	558	550	524	503	505	479
	0.0	0.07	7.6	21.9	65.0	89.8	97.3	98.4	100
390.1[b]	652	599	564	564	553	540	514	503	483
	0.0	0.005	8.1	15.5	61.6	83.7	94.9	97.4	100
393.2[a]	752	723	568	565	562	551	532	505	481
	0	0.01	35.2	39.0	57.7	72.3	89.5	98.7	100
393.2[b]	822	799	577	576	575	508	501	485	483
	0.0	0.08	43.8	58.1	64.3	97.9	98.7	99.1	100
High cooling rate									
390.1[a]	631	598	563	564	551	526	510	504	486
	0.0	0.06	7.8	18.9	65.8	89.9	96.8	98.4	100
390.1[b]	635	601	563	561	551	523	N/A	503	472
	0.0	0.004	4.1	7	63.61	90.1	N/A	97.3	100
393.2[a]	740	732	575	571	569	504.1	494.7	479	478
	0.0	0.12	30.2	31.0	62.5	96.5	97.1	98.2	100
393.2[b]	815	796	575	572	572	501	497	489	476
	0.0	0.05	45.5	56.0	65.2	98.93	99.1	99.6	100

DCP stands for Dendrite Coherency Point.

some cases, this difference is not too obvious and in general the fraction solid for the rest of the reaction was similar for the investigated solidification conditions.

Table 4 shows the cooling rates and apparent fraction solids for all the investigated alloys. Eq. (1) was used to determine the cooling rate.

$$\text{Cooling rate} = \frac{(T_{LIQ} - T_{SOL})}{(t_{SOL} - t_{LIQ})} (^{\circ}\text{C/s}) \quad (1)$$

where T_{LIQ} is the liquidus temperature (°C); T_{SOL} is the solidus temperature (°C); t_{LIQ} is the time recorded by thermal analysis at the liquidus temperature(s); t_{SOL} is the time recorded by thermal analysis at the solidus temperature(s).

The identification of the nucleation temperature for a particular phase was carried out by conducting a series of quenching experiments for the different alloys. Usually, the samples were quenched at the end of the growth of a particular phase, allowing a free coarsening for the phase itself. The quenched samples were then investigated using SEM/EDX to qualitatively determine their chemical composition and proceed with its stoichiometric identification as reported in the literature [4].

Table 4
Solidification conditions and cooling curve characteristics for the investigated alloys

Alloy	Cooling rate (°C/s)		Solidification range (°C)		Apparent fraction solid (%)	
	LCR	HCR	LCR	HCR	LCR	HCR
390.1[a]	0.08	0.7	121	112	10.6	10.1
390.1[b]	0.09	0.7	116	129	10.6	8.6
393.2[a]	0.31	1.2	242	254	8.2	8.2
393.2[b]	0.37	1.4	316	320	6.9	7.1

LCR and HCR stand for low and high cooling rates, respectively.

4. Characterization of rapidly solidified Al–Si hypereutectic alloys using LOM and SEM

Fig. 4 shows SEM and light optical micrographs for the 390.1[a,b] and 393.2[a,b] alloys that were quenched at different temperatures from above liquidus and during the mushy zone evolution and in the solid state. The presence of the Si agglomerates is of particular interest, since this confirms the existence of this phase at temperatures above the liquidus. Fig. 4 depicts micrographs with the phase identification conducted by SEM/EDX for the investigated alloys. In this figure, it is easy to identify the morphology for all the phases present in the microstructure of Al–Si hypereutectic alloys.

Fig. 4c–h shows the corresponding EDX spectra for the phases identified in the microstructure of the Al–Si hypereutectic alloys investigated in the present research. The EDX spectra for Mg and Fe enriched phases show the presence of Cu and Ni that is due to the vicinity of the phases, and their sizes combined with the interaction volume of the electron beam, i.e. the Mg_2Si phase was always found surrounded by Ni and Cu (Figs. 4 and 6).

In following are described the solidification pathways for the Al and Si enriched phases for the Al–Si alloys that are the two elements that provide the main characteristics and make them attractive for various automotive and aerospace applications. Al–Si hypereutectic alloys are dendrite free when are solidified under equilibrium conditions. The reason for this is that the first phase to solidify is Si followed by the Al–Si eutectic, which both are non-dendritic. At the industrial level, most alloys are solidified far from equilibrium conditions; for instance, Fig. 5 shows α-Al dendrites and/or haloes are formed in the Al–Si hypereutectic alloys following the "*skewed couple zone*" solidification [1]. In most cases, isolated dendrites are formed but usually they do not touch each other, they rather form a stage where a skeleton (identified in Table 3 as the "*Dendrite Coherency Point*")

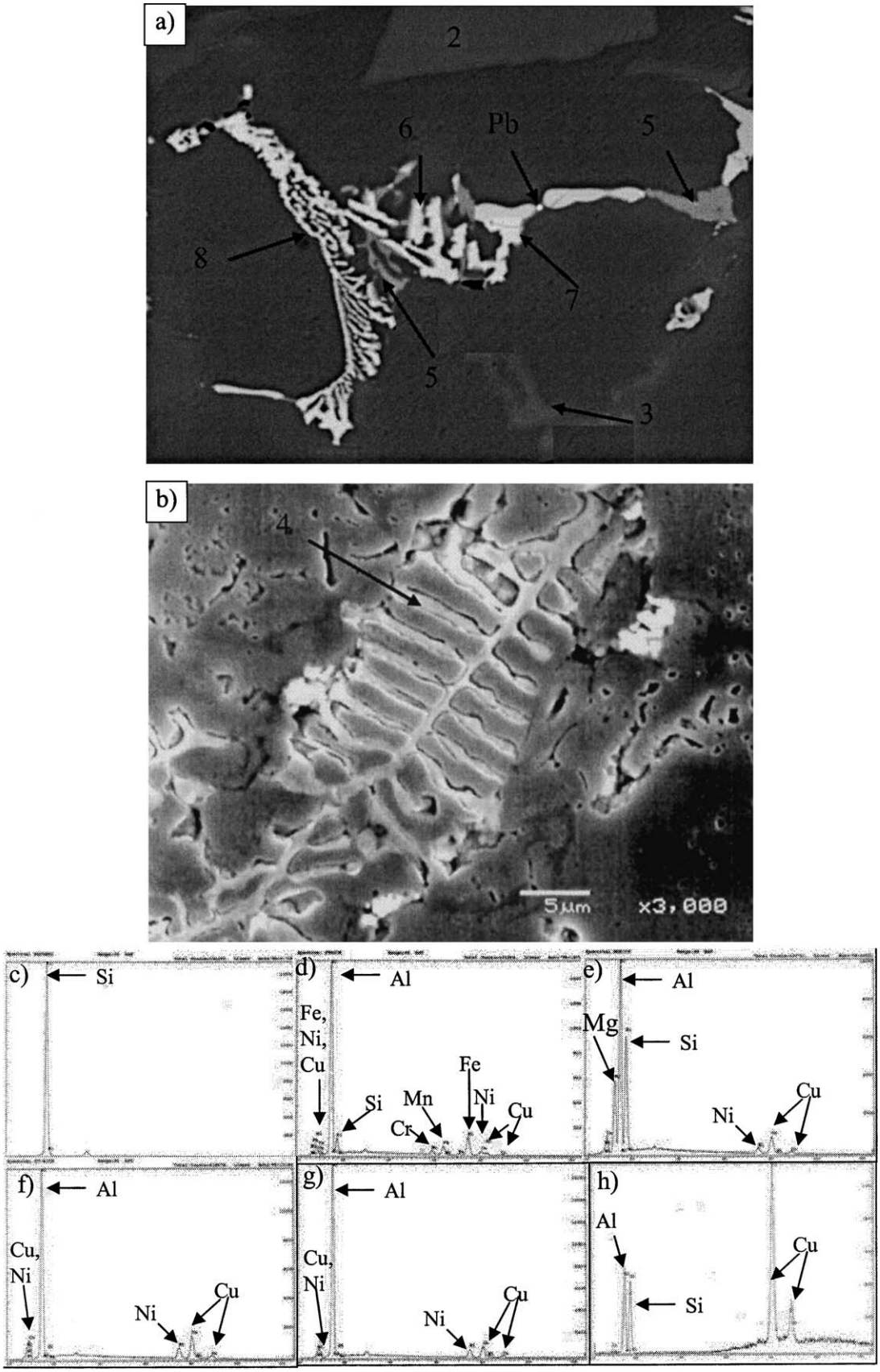

Fig. 4. SEM micrographs (a and b) showing the microstructure of samples fully solidified under natural heat exchange conditions showing the characteristic phases for the Al–Si hypereutectic alloys (for number identification, see Table 2). EDX results for the qualitative chemical analysis for the (c) Si, (d) $Al_{15}(Fe, Cr, Mn)_3Si_2$, (e) Mg_2Si, (f) Al_3Ni, (g) Al_3CuNi, (h) Al_2Cu.

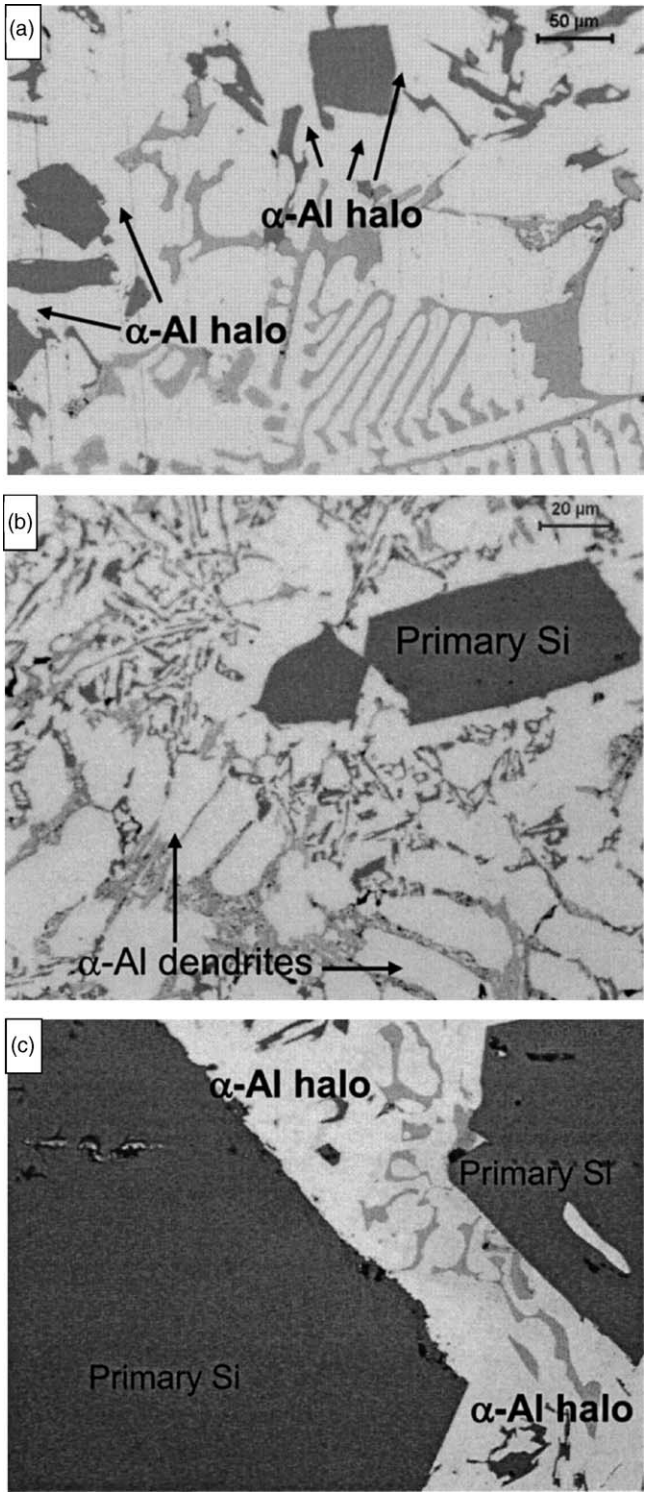

Fig. 5. Optical micrographs of the (a) 390.1[a], (b) 390.1[b] and (c) 393.2[b] alloys solidified at high cooling rates (0.7, 0.7 and 1.2 °C/s, respectively), showing the formation of the non-equilibrium phases (α-Al halo and dendrites).

is created. Fig. 5 shows examples of the α-Al haloes and α-dendrites present in the investigated alloys that were solidified far from equilibrium (high cooling rate). The so-called skeleton is formed by the primary Si, α-Al haloes, the α-Al dendrites and the Al–Si eutectic and increases the rigidity of the molten alloy.

The Fe-based phases can be found with various stoichiometries with the script type appearance (Al_8Fe_2Si, α-$Al_{12}Fe_3Si_2$, α-$Al_{15}(Fe, Cr, Mn)_3Si_2$, π-$Al_8Mg_3FeSi_6$ and the π-$Al_{15}Mg_8Cu_2Si_6$) [38]. However, based on the EDX spectrum (Fig. 4d), the presence of Cr and Mn lead the identification of the α-Al–Fe–Si type as α-$Al_{15}(Fe, Cr, Mn)_3Si_2$ as most probable stoichiometry. The Fe enriched phases are particularly important for the Al–Si hypereutectic alloys, since they are detrimental for the mechanical properties. However, in this research, the presence of Mn in the α-$Al_{15}(Fe, Cr, Mn)_3Si_2$ act as a modifier, promoting the transformation from needle-like (detrimental phase) into the Chinese script that is less detrimental (Fig. 4b). Fe is present in the investigated alloys as a sub product characteristic of secondary (recycled) alloys. Contrary, alloys such as 356 and 357 have non or negligible amounts of Fe, but are considerably more expensive.

At a temperature of ∼560 °C was identified as the last point for the coarsening for the primary Si particles and the beginning of nucleation of the Al–Si eutectic. At this temperature, some of the remaining molten alloy has a similar composition to the eutectic and some of the precipitating Al–Si particles have fine eutectic appearance. The 560 °C is a temperature close to the Dendrite Coherency Point, therefore, after this point, no apparent enlargement of the dendrites was supposed to occur, but they

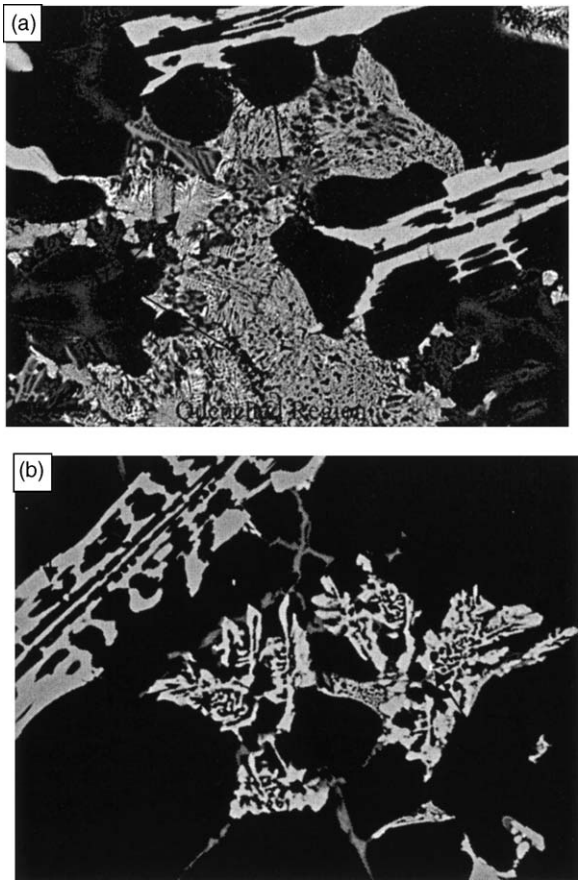

Fig. 6. SEM micrographs of the 390.1[a] alloy from the (a) edge and (b) centre of the analytical samples. The sample was quenched at 500 °C. Note the difference in morphology of the Al_2Cu indicating the presence of more than one phase particularly in the quenched sample.

continue coarsening by the interdendritic feeding. The Dendrite Coherency Point can be identified as the point where the semi-solid slurry becomes rigid, and there is no longer free flow of the remaining liquid, as the so-called skeleton starts forming and prevents the free flow of the remaining molten metal (see Fig. 3).

The Mg_2Si phase was identified in the sample quenched at a temperature of 550 °C that is ∼5 °C above the precipitation of this eutectic (∼545 °C) and has a very fine appearance characteristic of a partially solidified phase. In Fig. 6 can be observed the fine Mg_2Si particles surrounded by quenched Cu and Ni enriched regions.

At 525 °C, which is a temperature close to the nucleation of the Ni enriched eutectic such as the Al_3Ni. The 390.1[a] alloy used in this research has a Ni content of 2.19 wt.% which is unusual for alloys such as the 390.1 with a common Ni content of <0.5 wt.% Ni. The investigated 390.1 alloy was added extra Ni with the aim to be used for pistons where no precipitation hardening promoted by heat or solution treatments is carried out. This particular alloy after the artificial aging is characteristic for its high dimensional stability [5]. The characterization of the Ni rich phases presented in the 390.1[a] alloy were compared to the Ni phases present in the 339 Al–Si alloy which has similar Ni content and shows two Ni enriched phases (Al_3Ni, and Al_3CuNi) that were also identified in the 390.1[a,b] and 393.2[a,b] alloys (Figs. 4 and 6). The identification of Ni and Cu together for the Al_3Ni phase is due to the high similarity among both elements that based on the Hume–Rothery Empirical Rules they have total solubility (ideal solution) in the solid state. Therefore, the atoms of Cu and Ni for this phase could be interchangeable [43–45].

The Al–Cu enriched phases were identified at temperatures of 500 °C or below that was also the end of the dendritic coarsening. The SEM micrographs of this sample revealed that below 550 °C, this temperature the nucleation of the Al_3CuNi the Al_2Cu takes place. Fig. 7a shows SEM/BSE micrographs of the edge of the sample, which is the area that solidified, first as soon as the sample is in contact with the quenching media; this micrograph show after fully solidification the phases Mg_2Si, Al_3Ni and Al_3NiCu eutectics and it is clear that the Al_2Cu eutectic phase has a frozen-like (quenched) appearance. The analysis of the same sample in the centre shows the Al_2Cu eutectic phase after full solidification; actually, there are more than one phase with the Al_2Cu composition, but with different appearance (Fig. 6b) that confirms the results presented in references [4,37]. Therefore, it can be concluded that the Al_2Cu were the last phase to solidify for the 390.1 and 393.2 Al–Si hypereutectic alloys together with the low melting point elements (Fig. 6b).

The main factors that have effect on the microstructure are the chemical composition and solidification conditions, partic-

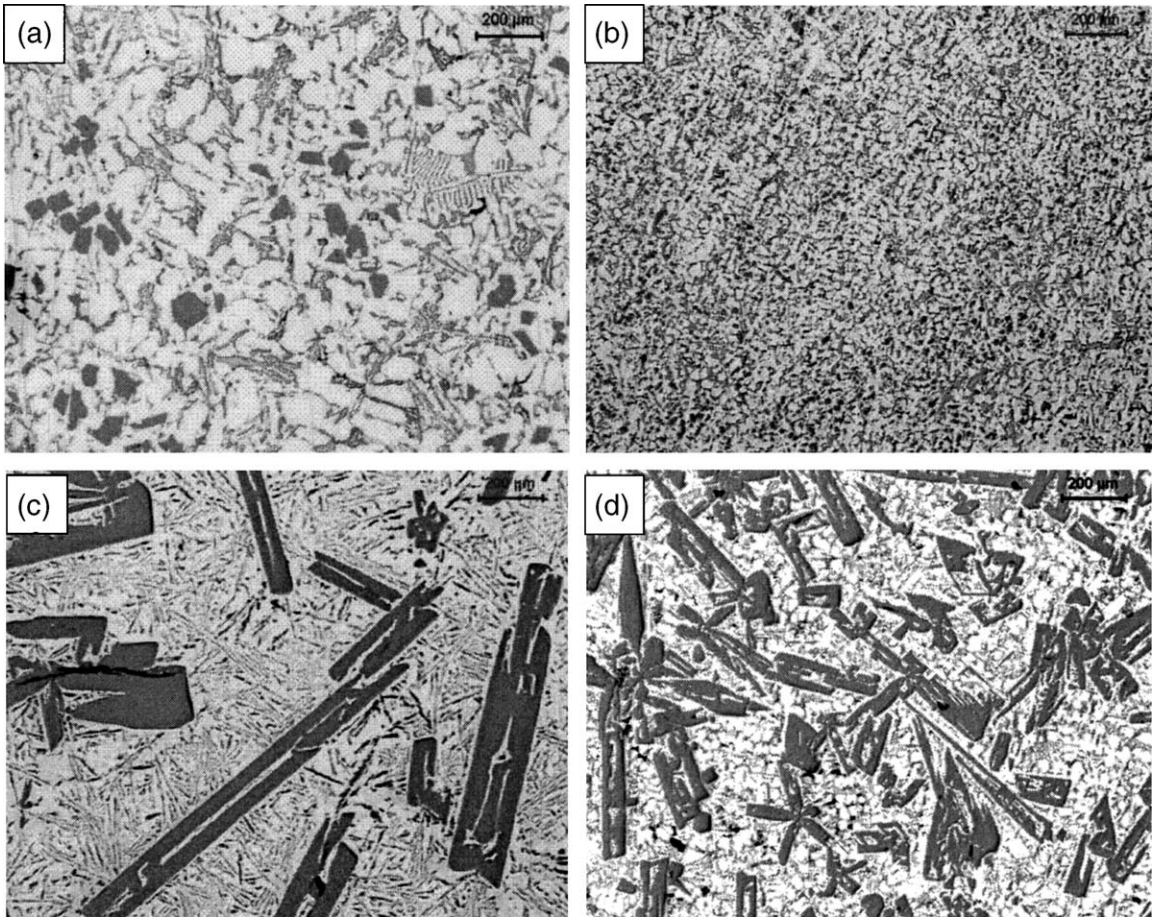

Fig. 7. Microstructure of the 390.1[a] (a and b) and 393.2[a] (c and d) Al–Si alloys solidified at the following cooling rates (a) 0.08 °C/s, (b and d) >5 °C/s and (c) 0.31 °C/s.

ularly, cooling rate and can be monitored by thermal analysis. Fig. 7 shows the microstructure of the 390.1[a,b] and 393.2[a] Al–Si hypereutectic alloys presenting the effect of the chemical composition as well as the cooling rate conditions. The cooling rate for the investigated samples presented in Fig. 7 was increased from 0.08 to >15 °C/s, which shows that alloy compositions such as the 390.1[a,b] are more sensible to the cooling rate than the 393.2[a,b] alloys. Therefore, for the industrial use of alloys such as the 393.2[a,b], their main limitation is the coarse primary Si particles that cannot be thermally or chemically fully modify and has the tendency to crack at even very low stress levels (i.e. during polishing) exposing the soft Al matrix to extreme wear. The effect of chemical modifiers for alloys with high Si (i.e. 393.2) is very limited [42]; therefore, other methodologies such as liquid and/or semi-solid state electromagnetic stirring and vibration melt treatments are suggested to refine phases and modify the microstructure drastically. In turn, mechanical and service characteristics such as wear and bulk hardness of these alloys will be increased abruptly [12].

Comparing the results in the present investigation, it can be confirmed that all phases detected by thermal analysis were identified using optical or electron microscopy. Fe and Pb rich phases were not detected by thermal analysis, but they were identified using optical and electron microscopy. Pb particles were observed under the SEM in backscattering mode at 1000× magnification as shown in Figs. 4 and 6. The Pb based particles are present in the Al–Si alloys as by-products of a secondary smelting process similarly to Fe [38].

5. Conclusions

A total of nine phases were detected using thermal analysis of microscopy. Particular reactions for the Si agglomerates can be identified using thermal analysis and in the microstructure of quenched samples using optical and electron microscopy. The Si agglomerates have a nucleation temperature higher to the superheat temperature of 150 °C used for the present research. A possible phase transformation was evident in the first derivative at temperatures higher than liquidus that could indicate a possible transformation from the Si agglomerate to the primary Si particles. The determination of the "*apparent fraction solid*" (af_s) can be used to develop an algorithm(s) capable for the prediction of the strengthening effect of Mg, Ni and Cu. The primary Si is more sensible to the high cooling rate in alloys with lower Si content (i.e. 390.1[a,b]). The ideal temperatures for the heat treatments is close to the end of solidification of the Cu enriched phases, which also correspond to the highest Cu solubility in the Al matrix, this would ideally maximize the strengthening effect of the Cu and Ni. The presence of Mn in the Fe enriched phases showed a strong modification effect from the *needle-like* structure to "*Chinese script structure*" that is less detrimental to the mechanical properties of Al–Si hypereutectic alloys.

Acknowledgements

Dr. F.C. Robles Hernaández would like to thank the National Science and Technology Council (CONACyT) in Mexico for financial assistance during his Ph.D. studies. The authors would like to express their appreciation to the Natural Sciences and Engineering Research Council of Canada (NSERC).

References

[1] J.E. Gruslezki, B.M. Closset, Microstructure Development During Casting, first ed., American Foundry Society Inc., Chicago, Il, 1990.
[2] J. Campbell, Castings, third ed., Butterworth-Heinemann, London, 2003.
[3] ASM Metals Handbook, vol. 2, Properties and Selection: Non-Ferrous Alloys and Special Purpose Materials, ASM International, 1990.
[4] L. Bäckerud. G. Chai. J. Tamminem, Solidification Characteristics of Aluminiums Alloys, vol. 2, American Foundry Society/SKANALUMINIUM, USA, 1990.
[5] A.G. Kolbemschmidt, 75 Years Kolbemschmidt, Brochure, September 1985, pp. 1–51.
[6] J.L. Jostard, Modern Casting, AFS Casting Congress, October 1971, pp. 71–76.
[7] J.P. Norbye, Automobile Eng. (1970) 320–326.
[8] R.E. Green, Die Casting Eng. (1970) 12–26.
[9] J.L. Jostard, 6th SDCE International Die Casting Congress, Cleveland, Ohio, November 1970, pp. 1–6.
[10] R. Francis, PhD Dissertation, University of Windsor, Windsor, 2005.
[11] L. Bäckerud, G. Chai, J. Tamminem, Solidification Characteristics of Aluminiums Alloys, vol. 3, American Foundry Society/SKANALUMINIUM, USA, 1990.
[12] F.C. Robles Hernandez, Ph.D. Dissertation, University of Windsor, 2004, p. 251.
[13] J. Sokolowski, J. Mazurek, AFS Trans. 95 (1987) 373–376.
[14] L. Lasa, J.M. Rodriguez-Ibabe, Mater. Sci. Eng. A 363 (2003) 193–202.
[15] T. Hejwowski, A. Weronski, Vacuum 65 (2002) 427–432.
[16] F.C. Robles Hernández, M. Kasprzak, J.H. Sokolowski, 43rd Conference of Metallurgists, Hamilton, Canada, August 2004, p. 583.
[17] G.K. Sigworth, M.M. Guzowski, AFS Trans. 93 (1985) 907–912.
[18] L. Heusler, F.J. Feukus, M.O. Otte, AFS Trans. 109 (2001) 215–223.
[19] W.D. Griffiths, D.G. McCartney, Mater. Sci. Eng. A 222 (1997) 149–157.
[20] L.A. Narayanan, F.H. Samuel, J.E. Gruzleski, AFS Trans. 100 (1992) 383–391.
[21] M. Kasprzak, W. Kasprzak, J.H. Sokolowski, Conference on Technology Transfer Partnership for the Development of the Aluminium Industry, McGill University, Montreal, Canada, September 2002.
[22] M. Kasprzak, W. Kasprzak, C.A. Kierkus, W.T. Kierkus, J.H. Sokolowski, Filling and Feeding of Castings, University of Birmingham, UK, 2002.
[23] M. Kasprzak, W. Kasprzak, W.T. Kierkus, J.H. Sokolowski, Proceedings of the 131st TMS Ann. Meet., Seattle, WA, February 2002, pp. 619–630.
[24] M. Kasprzak, W. Kasprzak, W.T. Kierkus, J.H. Sokolowski, Internal IRC Report, 2002.
[25] M. Kasprzak, W. Kasprzak, W.T. Kierkus, J.H. Sokolowski, Patent PCT/CA02/01903, Canada, 2002.
[26] W.T. Kierkus, J.H. Sokolowski, AFS Trans. 107 (1999) 161–167.
[27] W.T. Kierkus, J.H. Sokolowski, AFS Trans. 14 (1999) 173–179.
[28] I.G. Brodova, P.S. Popel, G.I. Eskin, Advances in Metallic Alloys, Fridlyander and Eskin, New York, 2000, Chapters 1 and 2.
[29] W. Weimin, X. Bian, J. Qin, S.I. Syliusarenko, Met. Mater. Tans. A 31A (2000) 2163–2168.
[30] M. Inui, S. Tadeda, Y. Shirakawa, S. Tamaki, Y. Waseda, Y. Tamaguchi, J. Phys. Soc. Jpn. 60 (1991) 3025–3031.
[31] B. Sadig, M. Dzugutov, S.R. Elliot, Phys. Rev. B 59 (1) (1999) 1–4.
[32] B. Xiufang, W. Weimin, Q. Jimgyu, Mater. Charac. 46 (2001) 25–29.
[33] M.D. Nave, A.K. Dahle, D.H. StJohn, Acta Mater. 50 (2002) 2837–2849.
[34] W. Weimin, X. Bian, J. Qin, J. Mater. Sci. Lett. 19 (2000) 1583–1585.
[35] X. Bian, W. Weimin, Mater. Lett. 44 (2000) 54–58.
[36] F.C. Robles Hernandez, M.B. Djurdjevic, W.T. Kierkus, J.H. Sokolowski, Mater. Sci. Eng. A 1–2 (2005) 271–396.
[37] M.B. Djurdjevic, W. Kasprzak, C.A. Kierkus, W.T. Kierkus, J.H. Sokolowski, AFS Trans. (2001) 517–528.

[38] R.I. Mackay, University of Windsor, Windsor, Ontario, Canada, PhD Dissertation, 2003, p. 287.
[39] M. Djurdjevic, H. Jiang, J. Sokolowski, Mater. Charac. 46 (2001) 31–38.
[40] B.D. Cullity, Elements of X-Ray Diffraction, Addison-Wesley Publishing Company Inc., 1978.
[41] A.K. Dahle, L. Arnberg, Acta Mater. 45 (2) (1997) 547–559.
[42] D. Apelian, G.K. Sigworth, K.R. Whaler, AFS Trans. (1984) 297–307.
[43] http://bguy.mse.uiuc.edu/Matere200/Handouts/Hume-Rothery.pdf, as posted in 6 May 2004.
[44] http://cyberbuzz.gatech.edu/asm_tms/phase_diagrams/pd/cu_ni.gif, as posted in 6 May 2004.
[45] R.T. DeHoff, Thermodynamics in Materials Science, First ed., Mc. Graw-Hill, 1993, Chapter 8.